Applied Catalysis B: Environmental 218 (2017) 208–219

Contents lists available at ScienceDirect

Applied Catalysis B: Environmental

journal homepage: www.elsevier.com/locate/apcatb

Research Paper

Facile *in-situ* design strategy to disperse TiO_2 nanoparticles on graphene for the enhanced photocatalytic degradation of rhodamine 6G

Pu Shengyan[a,b,*,1], Zhu Rongxin[a,1], Ma Hui[a], Deng Daili[a], Pei Xiangjun[a], Qi Fei[c,**], Chu Wei[b,**]

[a] State Key Laboratory of Geohazard Prevention and Geoenvironment Protection (Chengdu University of Technology), 1#, Dongsanlu, Erxianqiao, Chengdu 610059, Sichuan, PR China
[b] Department of Civil and Environmental Engineering, The Hong Kong Polytechnic University, Hong Kong, PR China
[c] College of Environmental Science and Engineering, Beijing Forestry University, Beijing 100083, PR China

ARTICLE INFO

Article history:
Received 4 April 2017
Received in revised form 29 May 2017
Accepted 14 June 2017
Available online 17 June 2017

Keywords:
Graphene oxide
TiO_2
Photocatalysis
In-situ design
Photodegradation
Dye wastewater

ABSTRACT

Photogenerated electron/hole recombination greatly limits the catalytic efficiency of TiO_2, and recently modification with graphene substance has been regarded as an effective way to enhance the photocatalytic performance of TiO_2. When referring to the fabrication of graphene based materials, the reduction process of graphene oxide has been demonstrated to be a key step. Therefore, it is highly required to develop an efficient and simple route for the GO reduction and the formation of TiO_2@rGO composites. In this study, we have demonstrated a facile and environmentally friendly strategy for *in-situ* preparation of the TiO_2@rGO "dyade" hybrid and systematically investigated the photodegradation efficiency of the resultant composite by utilizing rhodamine 6G as the model pollutant. The obtained TiO_2@rGO has a significant enhancement in photo energy adsorption leading to the effective photocatalytic degradation reactions. The results indicated that the best performance was conducted by the TiO_2@rGO (10 wt%, 120 min's irradiation), which exhibited more than triple the higher photodegradation rate than commercial TiO_2 (P25) nanoparticles mainly due to two aspects, the rapid separation of h^+/e^- and to improve adsorption. This work provides new insight into the synthesis of TiO_2@rGO composites as a high performance photocatalyst for the degradation of organic contaminant.

1. Introduction

Recently, the photocatalytic process for dye containing wastewater degradation has attracted considerable attention. Among a great number of semiconductors, TiO_2 has been identified as one of the most promising photocatalysts which expects to play an important role in environmental remediation [1,2], solar energy [3] and other fields [4,5], due to its nontoxicity, low cost, abundant resources and high catalytic efficiency [6]. However, fast h^+/e^- recombination greatly limits the practical application of TiO_2 [7], and various attempts have been applied to improve the catalytic efficiency of TiO_2 in recent decades. For example, Zhang et al. [8] reported that boron-doped TiO_2 with a tunable anatase/rutile ratio, obtained through a simple one-step calcination method using titanium and boron mixture as the precursor, showed more than 4 times higher reaction rate in atrazine degradation than the bare TiO_2 nanoparticles. Wang et al. [9] demonstrated that the degradation rate of rhodamine B could be improved to 7.2 times by combining with the g-C_3N_4 via a facile calcination method using tetrabutyl titanate and melamine as the feedstocks. Recently, modifying TiO_2 with carbonaceous substances, such as carbon nanotubes (CNTs) and graphene which have large specific surface area and high carrier mobility, is regarded as an effective strategy to further enhance the photocatalytic performance of TiO_2 [10–12].

Among various carbonaceous materials, graphene, which was discovered as a one-atom-thick sheet composed of sp^2-hybridized carbon atoms in a hexagonal lattice, is rapidly gaining interest from a wide spectrum of research fields. This is mainly due to its extraordinary physicochemical properties [13,14], such as remarkable

* Corresponding author at: State Key Laboratory of Geohazard Prevention and Geoenvironment Protection (Chengdu University of Technology), 1#, Dongsanlu, Erxianqiao, Chengdu 610059, Sichuan, PR China.
** Corresponding authors.
E-mail addresses: pushengyan@gmail.com, pushengyan13@cdut.cn (S. Pu).
[1] Contributed equally to this work.

http://dx.doi.org/10.1016/j.apcatb.2017.06.039
0926-3373/

mechanical strength, high thermal conductivity (5000 $Wm^{-1} K^{-1}$), outstanding electron mobility (250,000 $cm^2 V^{-1} s^{-1}$) and specific surface area (2630 $m^2 g^{-1}$).

To combine the advantages of both TiO_2 and graphene, the resultant composites could not only hinder the recombination of h^+/e^- by transferring the photoexcited electron to graphene surface, but also further enhance the surface area of TiO_2 for better adsorptive properties [15]. Therefore, numerous efforts have been paid to integrate TiO_2 with graphene for the photodegradation efficiency improvement. Recently, various methods [16–18], such as physical mixing, hydrothermal, electrochemical deposition, sol-gel and self-assemble approaches, have been applied to form TiO_2/graphene nanocomposites. For example, Zhang et al. [19] reported that a physical mixing of P25 and graphene composite was obtained through a hydrothermal method, which shows enhanced adsorption and photocatalytic degradation of methylene blue imitated wastewater. Liang et al. [20] demonstrated that TiO_2/graphene composites produced by hydrolysis and hydrothermal treatments showed 110% improved photodegradation efficiency over pure TiO_2. However, these traditional strategies have their inevitable shortcomings, such as involvement of toxic reductive agents (eg. N_2H_4, $NaBH_4$), requirement of high pressure/temperature (>500 °C), additives of acid/alkali, time- and energy-consuming. Therefore, their practical applications have been limited.

In 2008, Kamat et al. [21] demonstrated a facile and chemical free strategy to effectively reduce graphene oxide (GO) sheets through an on-demand UV-assisted methodology. Furthermore, during the reduction process, the photoactive TiO_2/graphene composites could be simultaneously synthesized either. However, the practical application of the as-prepared TiO_2@rGO composites has not been systematically studied and the preparation conditions need further optimization to enhance its catalytic performance.

In this paper, TiO_2@rGO composites have been successfully synthesized through a facile *in-situ* UV-assisted photoreduction method. Then, by regulating the GO dosage and irradiation duration, the relationship between the reduction degree of GO and the photocatalytic efficiency of the reluctant complex has been investigated using rhodamine 6G (Rh 6G) as the target contaminant. Furthermore, for practical application, the performance of the resultant composites in simulated dye wastewaters with different pH value have been investigated. The results illustrate that the obtained TiO_2@rGO composite is able to absorb a high amount of photo energy and drive effectively photodegradation reactions. This work may provide a facile, promising, and environmentally friendly strategy for the large-scale preparation of graphene-based composite materials.

2. Experimental

2.1. Materials

Sulfuric acid (H_2SO_4, 98 wt%), ammonium hydroxide ($NH_3{\cdot}H_2O$), potassium hypermanganate ($KMnO_4$), hydrogen peroxide (H_2O_2, 30 wt%), hydrochloric acid (HCl, 37 wt%), absolute ethanol (C_2H_6O) were all of analytical grade. All of the chemicals above were obtained from Chengdu Kelong Chemical Reagent Company (Sichuan, China) and used as received without further purification. Graphite powder (purity > 99.95%) was purchased from Aladdin Industrial Corporation (Shanghai, China). TiO_2 (P25) nanoparticles powder was supplied by Degussa Company (Germany). Rhodamine 6G was obtained from Sigma-Aldrich. Deionized (DI) water used for all experiments was generated from Milli-Q water purification system (Ulupure Corporation).

2.2. Synthesis of graphene oxide

The graphene oxide was synthesized from natural graphite powder (99.95%) by the modified Hummers method [22]. In a typical synthesis, the producing procedure was as followed: (1) the graphite powder (2.0 g) and sodium nitrate (1.2 g) were put into a round-bottom flask. Then, 60 mL concentrated H_2SO_4 was added dropwise. The resultant dark blue mixture was further treated with ultrasonic, and then was placed into an ice bath apparatus and allowed for intensive mixing using magnetic stirrer. (2) Subsequently, potassium hypermanganate (8.8 g) was slowly added and the mixture was stirred for 12 h. During the processing, an ice bath should be utilized to avoid the temperature exceeding 20 °C. (3) Then, 72 mL distilled water was carefully added, and the temperature should be maintained under 20 °C until the instillment was terminated. The mixture was continuously stirred at 50 °C for another 12 h. (4) After that, the reaction temperature was regulated to 35 °C and stirred for another 12 h untill the color of the mixture was changed from yellowish-brown colour to bright yellow colour. Then, 22 mL H_2O_2 was slowly added and the resultant mixture was stirred for 3 h, resulting in plenty of bubble formation. (5) Finally, the mixture was washed by 5% HCl solution and ethanol by turns until the pH value of supernate became neutral, and the initial product was dispersed in absolute alcohol by sonication.

2.3. Synthesis of TiO_2@rGO composite

The synthesis of TiO_2@rGO nanocomposite was conducted simultaneously with the photoreduction of GO nanosheets in a simple GO/TiO_2 ethanol system. Commercial TiO_2 nanoparticles (P25), a well-known commercial photocatalyst with high catalytic activity and good dispersion, was pretreated in furnace at 500 °C for 2 h to remove the adsorbed substances and keep a clean surface.

In a typical synthesis, the producing procedure was as followed: (1) firstly, the prepared GO solution was diluted by absolute ethanol and the concentration would be regulated at 0.5 mg/ml. (2) Then, 0.7 g TiO_2 powder was added in 70 mL above GO/ethanol solution under continuous stirring at room temperature to obtain a milky suspension. (3) After stirring, the mixture was treated by ultrasound for 30 min to form a homogeneous flaxen suspension solution and to make GO sufficiently contact with TiO_2 nanoparticles. (4) Then, the resultant mixing solution was bubbled with nitrogen to remove the dissolved oxygen and further disperse the TiO_2 nanoparticles in solution. (5) After bubbling for 30 min, the suspension was irradiated under UV condition. With increasing irradiation time, the color of the suspension gradually changed from flaxen to black, suggesting the effective reduction of GO to rGO. (6) Finally, the obtained mixture was dried at 60 °C for 12 h to obtain the TiO_2@rGO nanocomposites.

The weight ratio of GO to TiO_2 would be regulated at 0, 0.5, 1, 2, 5, 10 wt%. The irradiation duration was controlled to 5, 15, 30, 60, 120 min, respectively. A 300W mercury lamp equipped with a cutoff filter (providing UV light with $\lambda \leq 400$ nm) was used as an excitation light source.

2.4. Characterizations

Transmission electron microscopy (TEM) observations were performed on a JEM-2100 TEM system (JEOL, Tokyo Japan) at an acceleration voltage of 200 kV. The composition and crystallinity of the samples were characterized by X-ray powder diffraction patterns (XRD) on a DX-2700 X-Ray diffractometer using *Cu-Kα* radiation (λ = 1.540562 Å, 40 kV, 30 mA) as the X-ray source at a scanning rate of 3°/min in the range of 3° to 80°. XPS measurements were performed using a *K-Alpha* Probe (Thermo Scientific, USA) with a monochromated *Al-Kα* radiation (300 W). Fourier Trans-

form Infrared spectra (FTIR) were acquired using a Spectrum 6700 FTIR spectrometer (Nicolet, America). TGA was performed under an air flow (50 mL/min) using a TA Instruments TGA- STA 449F3 (NETZSCH, Germany) and the samples were heated from room temperature to 1000 °C at 10 °C/min. UV–vis spectra was obtained on a spectrophotometer (Shanghai United Instrument Co., Ltd, China). The photoluminescence (PL) excitation and emission spectra were measured on a LabRAM HR Evolution raman microscopes (HORIBA Scientific, France). Electron paramagnetic resonance spectra (EPR) was preformed on a EMX-8 spectrometer (Bruker BioSpin Corp., Germany).

2.5. Photocatalytic experiments

The catalytic performances of as-synthesized TiO_2@rGO composites were evaluated by the commercial TiO_2 nanoparticles P25 as reference. The liquid-phase photocatalytic activity of each sample was evaluated in terms of the degradation of Rh 6G with an initial concentration of 20 mg/L. A 300W mercury lamp with a cut-off filter (λ > 400 nm) was used as light source and the reactor was cooled by running water to maintain the temperature at 25 °C. In photocatalytic degradation process, the pH of dye wastewater was adjusted to 3–11(±0.1) with 0.1 M H_2SO_4/NaOH before start-up without further adjustment during the reaction. Then, the catalyst (70 mg) was added into 70 mL Rh 6G solution, after ultrasonic dispersion, the suspensions were stirred in the dark for 2 h in order to establish the adsorption-desorption equilibrium. For a given time interval, 1 mL of the mixture solution was centrifuged at 8000 rpm for 5 min to get a supernatant liquid, leaving the catalysts as the precipitate. Furthermore, the concentrations of Rh 6G was determined from the maximum absorption (λ = 530 nm) by UV–vis spectrophotometer. Each result was a mean of three replications.

3. Results and discussion

3.1. Preparation of catalyst

The TiO_2@rGO composites were synthesized through an *in-situ* UV-assisted photoreduction strategy, as expressed in Fig 1a.

The color of TiO_2 alcohol blend was changed from semitransparent ivory to increasingly beige after instilling GO solution. Then, the ecru suspension was formed after sufficient stirring, which was recognized as GO/TiO_2/ethanol mixture. During the illuminated period, as UV irradiation duration extended, the mixture colour gradually turned from initial ecru to grey, and finally changed to black, which was due to the photogenerated electrons in TiO_2conduction band (CB) were produced and transformed GO to rGO through reduction [23].

$$TiO_2 + hv \rightarrow TiO_2\left(h^+ + e^-\right) \rightarrow TiO_2\left(e^-\right) + C_2H_4OH + H^+$$

$$TiO_2\left(e^-\right) + Graphene\ Oxide\ \ (GO) \rightarrow TiO_2@rGO\ composites$$

Furthermore, the color change has been suggested as partial restoration of the network within the carbon structure and witnessed through chemical reduction of the GO sheets [24,25]. Therefore, during the process, GO could be reduced to reduced graphene oxide (rGO), and TiO_2 nanoparticle would be simultaneously dispersed and bonded into it [21].

3.1.1. XRD characterization

As two main factors in TiO_2@rGO nanocomposites synthesizing process, the impacts of weight doping ratio and UV-irradiation duration were studied. In view of mild experimental conditions, the crystal structure of TiO_2 precursor could be well preserved based on the XRD results, as expressed in Fig. 2. It was evident that the obtained nanocomposites exhibited similar XRD patterns. The diffraction peaks for all samples matched well with the anatase TiO_2 (JCPDS Card No. 21-1272) and rutile phase (JCPDS Card No. 21-1272). Specifically, the peaks at 2θ values of 25.2°, 37.7°, 48.0°, 53.8°, 55.2°, 62.7°, 68.9°, 70.3°, and 75.1° could be indexed to (101), (004), (200), (105), (211), (204), (116), (220), and (215) crystal planes of anatase phase respectively. Furthermore, characteristic diffraction peaks at 27.5° and 36.1° could be observed either, which were attributed to the (110) and (101) faces of rutile phase.

In comparison with the bare TiO_2, it was easy to observe that the weight doping ratio and the irradiation duration in the TiO_2@rGO nanocomposites had little influence on the characteristic peaks of TiO_2. As illustrated in Fig. 2, the typical diffraction peaks of GO and rGO could hardly be found in the corresponding nanocomposites (as expressed in Fig. S1), which could be ascribed to the following

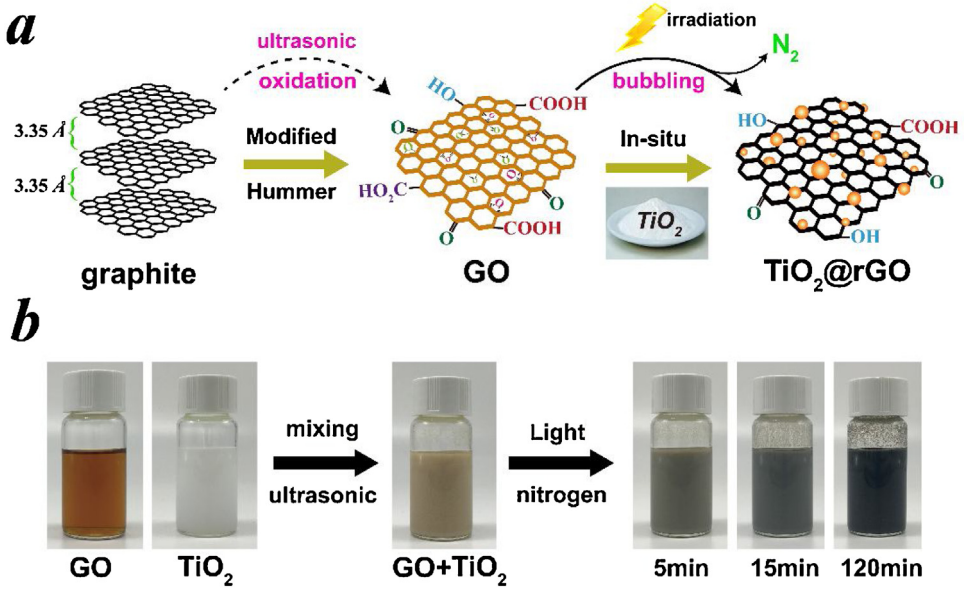

Fig. 1. (a) Schematic illustration of green synthesis of TiO_2@rGO composites by means of the *in-situ* UV-assisted photoreduction strategy; (b) Photographs of GO solution, TiO_2 suspension, the mixing solution and the obtained solution after 5, 15 and 120 min irradiation, respectively. (For interpretation of the references to colour in this figure legend, the reader is referred to the web version of this article.

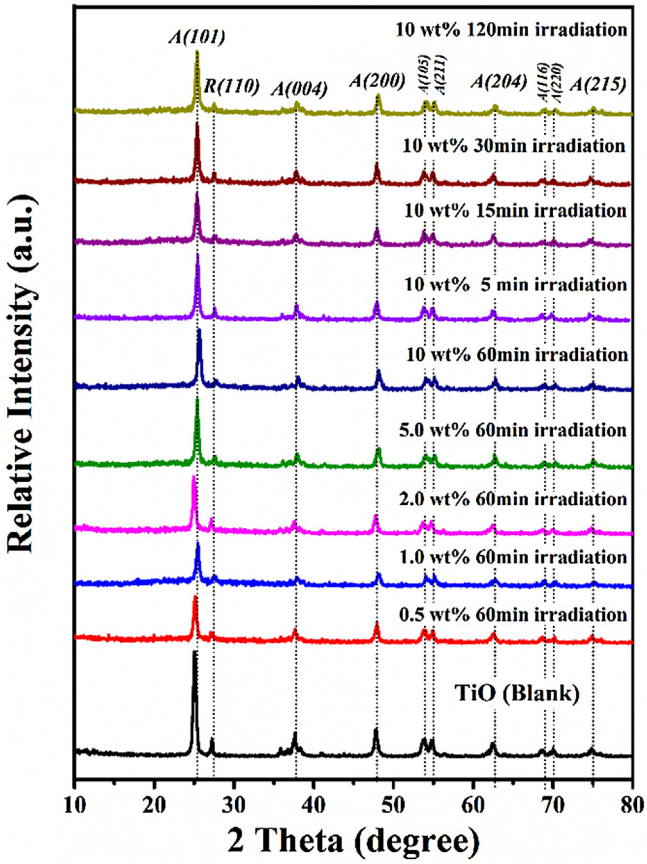

Fig. 2. XRD patterns of the TiO_2@rGO nanocomposites, in which A is anatase phase and R is rutile phase.

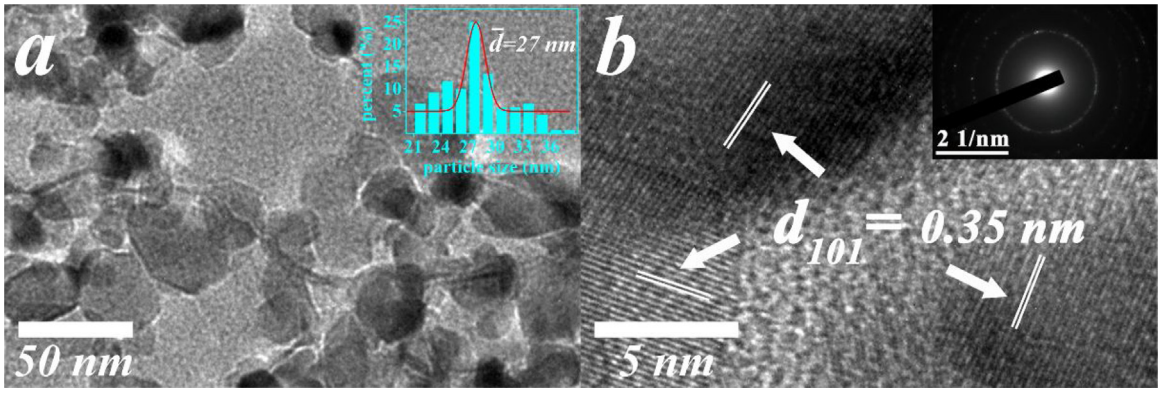

Fig. 3. (a) TEM and (b) HRTEM images of the TiO_2@rGO composites (10 wt%, 120 min irradiation).

three reasons. First of all, the trace amount of loaded GO and rGO could not be resolved by XRD. Then, no GO characteristic peaks found revealed that GO has already been reduced during the *in-situ* preparing process. Furthermore, the main peaks of reduced graphene oxide at 25° were probably shadowed and overlapped by the strong (101) peakof anatase TiO_2 at 25.3°, which is consistent with the previous reports [26]. Besides, the broadened diffraction peaks suggested that the nanocrystals were small in size. According to the Scherrer formula, the average crystallite size could be calculated to be approximately 26 nm.

3.1.2. TEM

The TEM images of TiO_2@rGO composites were shown in Fig. 3a–b which demonstrated the typical morphology and inner structure of the obtained compounds.

The semitranslucent graphene nanostructures can be observed owing to its ultrathin sheet like nature and TiO_2 was founded to be composed of many small nanoparticles with an average diameter of ~27 nm (Fig. 3a, inset) which perfectly fitted the computation from XRD. As for TiO_2@rGO composites, the surface of TiO_2 nanoparticles was mostly covered by rGO nanosheets, leading to the formation of an interconnected network. Besides, Fig. 1b illustrated the highresolution TEM (HR-TEM) observation which revealed that the graphene sheet was intensively covered by a dense layer of TiO_2 nanoparticles well crystallized with a *d*-spacing of 0.35 nm which was well matched to the d_{101} of anatase TiO_2. The corresponding SAED pattern (Fig. 3b, inset) of TiO_2@rGO composite further disclosed its polycrystalline feature, which was also consistent with the XRD result. These results suggested that the TiO_2 nanoparticles were effectively loaded on rGO sheets.

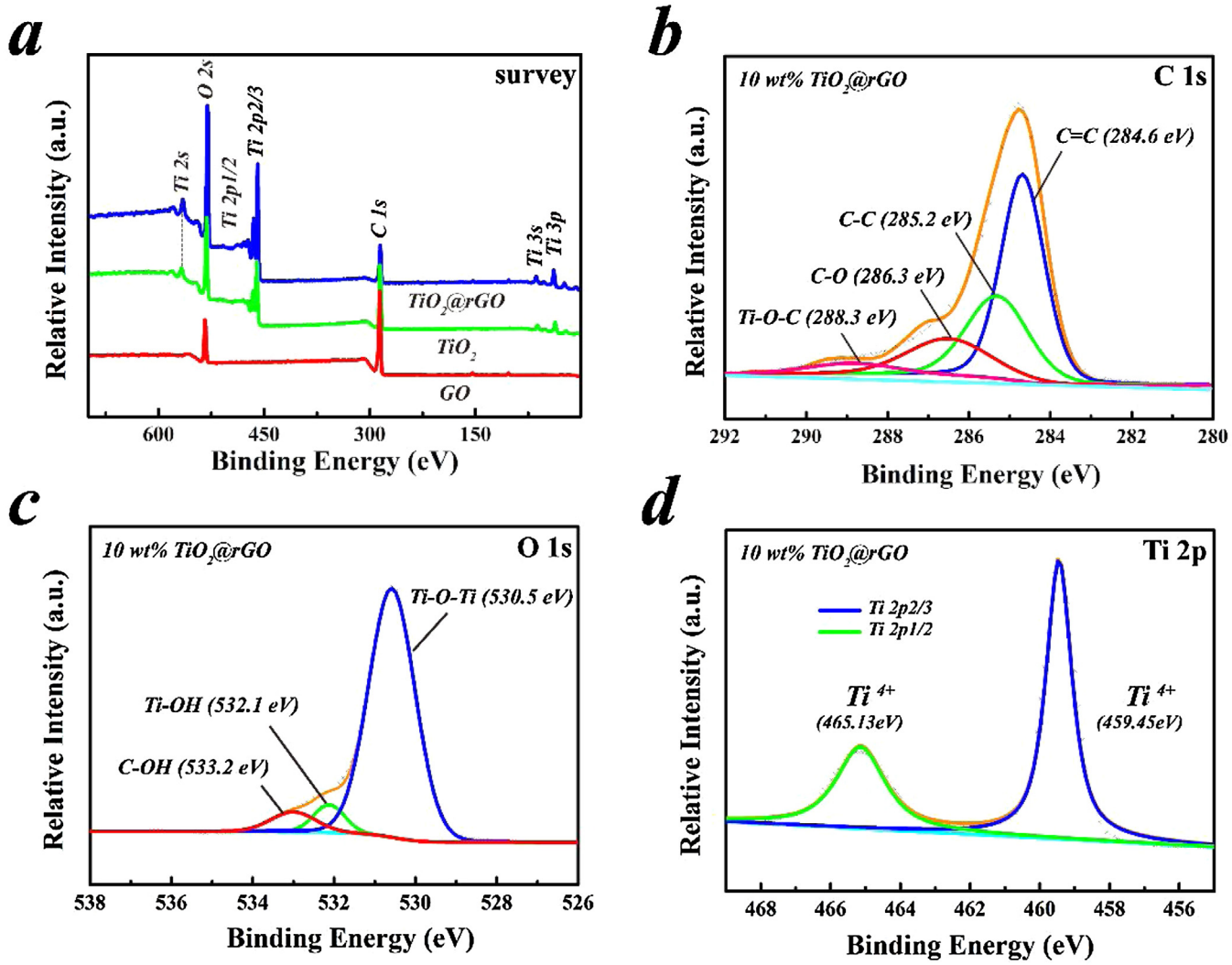

Fig. 4. The survey spectrum (a), C1s(b), O1s(c) and Ti2p(d) XPS spectra of the TiO_2@rGO composites (10 wt%, 120 min irradiation).

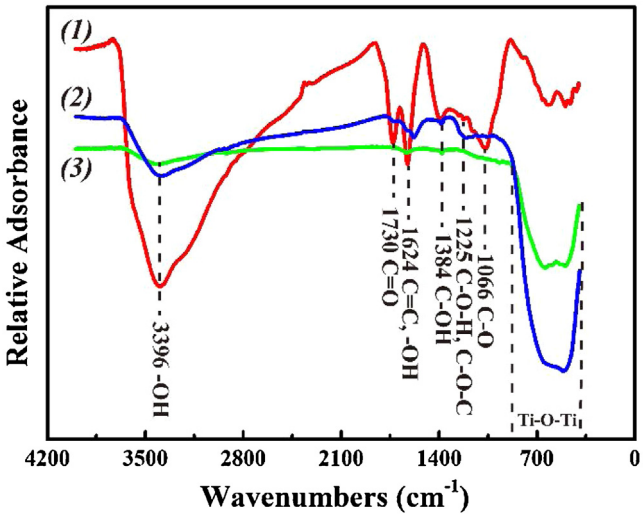

Fig. 5. FTIR spectra of (1) GO, (2) TiO_2, and (3) TiO_2@rGO composites (10 wt%, 120 min irradiation).

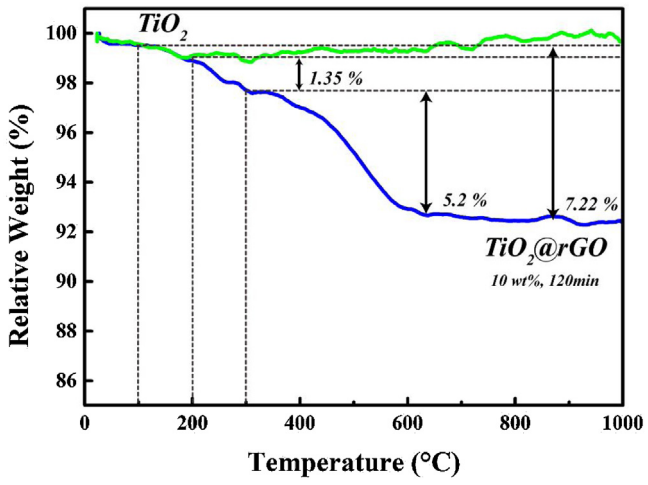

Fig. 6. TG analysis of TiO_2 and TiO_2@rGO composites (10 wt%, 120 min irradiation).

3.1.3. XPS

Through XPS test, the chemical states of elements in 10 wt% TiO_2@rGO nanocomposites were analyzed. According to Fig. 4a, the spectra indicated the existence of Ti, O, and C with the chemical binding energies of Ti 2*p*3/2 (459.45 eV), O 1 s (529.0 eV), and C 1 s (287.7 eV), respectively. It is necessary to consider its formation due to using of GO and TiO_2.

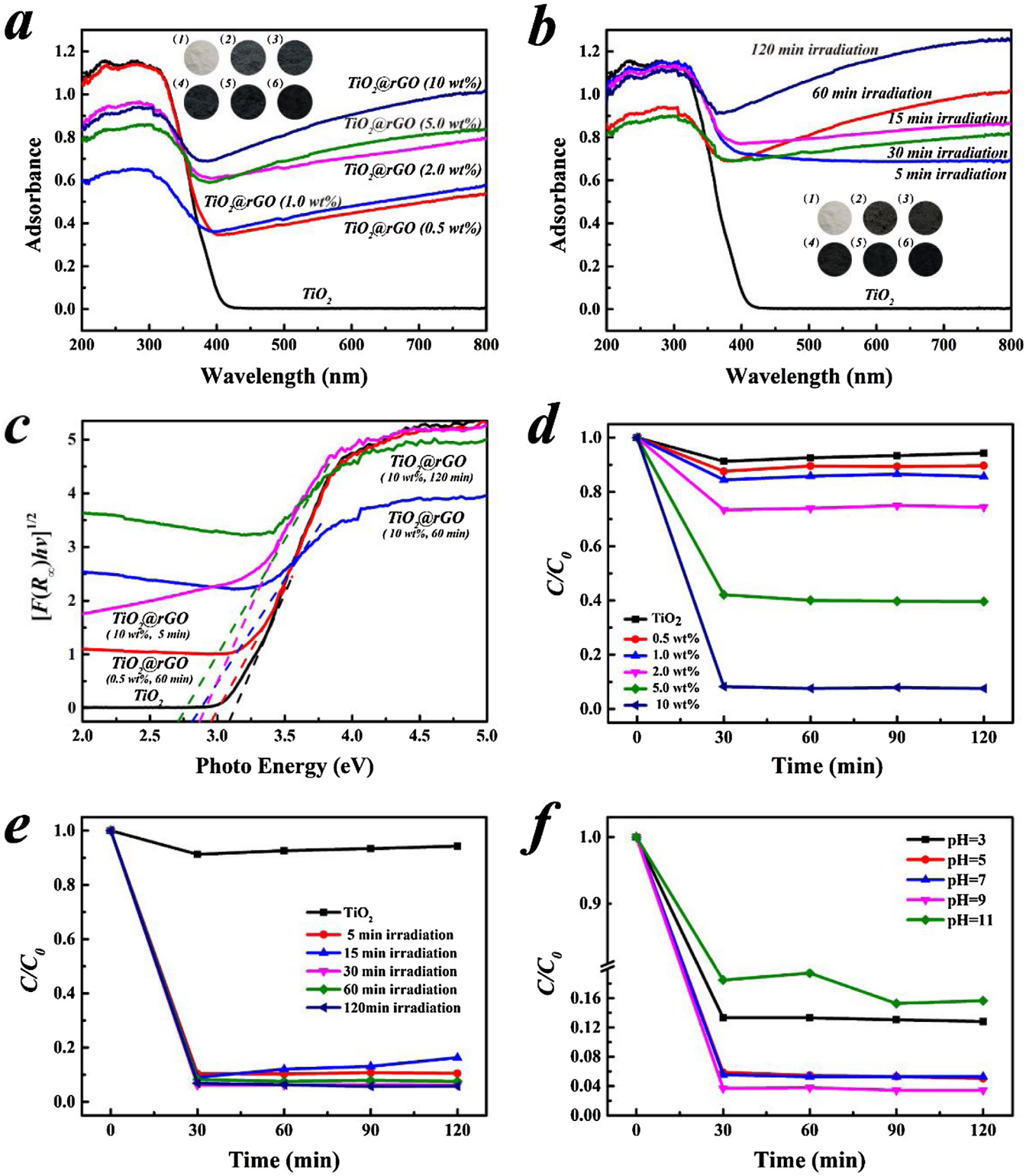

Fig. 7. (a) UV–vis diffuse spectra of TiO_2@rGO in different doping ratio (1) TiO_2, (2) 0.5 wt%, (3) 1.0 wt%, (4) 2.0 wt%, (5) 5.0 wt%, (6) 10 wt%; (b) UV–vis diffuse spectra of TiO_2@rGO(10 wt%) with different irradiation duration (1) TiO_2, (2) 5 min, (3) 15 min, (4) 30 min, (5) 60 min, (6) 120 min; (c) curve of $[F(R_\infty)h\nu]^{1/2}$ versus photon energy of pure TiO_2 and the prepared TiO_2@rGO composites; and the adsorption behavior of rhodamine 6G on the TiO_2@rGO with different doping ratio (d), various UV irradiation duration (e), and a series of initial pH (f), respectively.

Firstly, as shown in Fig. 4b, the C 1 s XPS signal of 10 wt% TiO_2@rGO compound showed four characteristic components. The main peak was dominated by elemental carbon at 284.6 eV, attributed mainly to sp^2 hybridized carbon (binding energy = 284.6 eV). Two weak peak at 285.2 and 286.3 eV were mainly attributed to sp^3 hybridized carbon and the oxygen bound species C–O, and the peak at 288.3 eV was assigned to Ti–O–C, respectively [27]. The presence of the Ti–O–C structure revealed that the C atoms have substituted some of the Ti atoms in the TiO_2 lattice during the preparation process and TiO_2@rGO have been

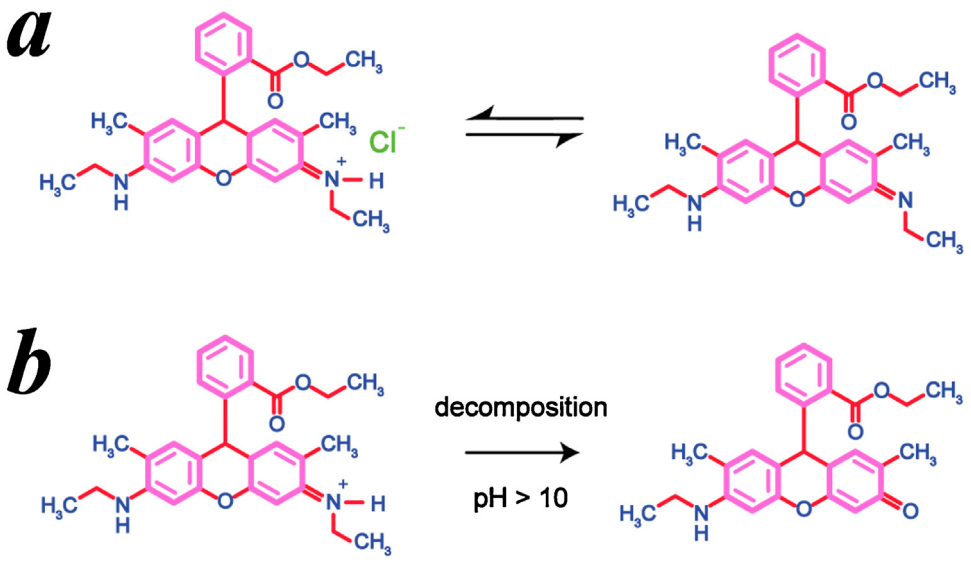

Fig. 8. (a) Molecular structure of rhodamine 6G (Rh 6G); (b) Scheme of onium ion transformation in strong alkaline condition.

formed after the *in-situ* strategy. Then, according to the high resolution spectra of O 1 s in Fig. 4c, it could be divided into three peaks: Ti–O–Ti bond (530.5 eV), Ti–OH bond (532.15 eV), C–OH and/or C–O–C species (533.2 eV) [28], respectively. Finally, as expressed in Fig. 4d, the binding energy of Ti(2*p*3/2) was 459.45 eV higher than pure TiO_2 (459 eV), this might be due to the C doped into TiO_2 led to an upward shift of Ti(2*p*3/2) and the formation of TiO_2@rGO. On the base of above discussion, it was reasonable to conclude that the successful synthesis of TiO_2@rGO via UV-assisted photoreduction process, as well as the Ti–O–C which made composites connect more closely.

3.1.4. FTIR

The reduction of GO to rGO could be further demonstrated through FTIR analysis, which expressed in Fig. 5. It illustrated that the curve of GO (Fig. 5-1) revealed many strong absorption peaks corresponding to various oxygen functional groups[29–31], such as water –OH stretching (3396 cm^{-1}), carboxylates or ketones C=O stretching (1730 cm^{-1}), water –OH bending, C=C stretching (1624 cm^{-1}), alcoholic C–OH bending (1384 cm^{-1}), epoxide C–O–C or phenolic C–O–H stretching (1225 cm^{-1}), and C–O stretching (1066 cm^{-1}).

For the pure TiO_2 (Fig. 5-3), the absorption peaks at 3396 cm^{-1} came from the water –OH group, whereas the wide peaks at 400–900 cm^{-1} was due to the stretching vibration of Ti–O–Ti bonds in crystalloid TiO_2 nanoparticles [32]. Then, after the UV-assisted *in-situ* photoreduction process, the intensity of absorption peaks corresponding to oxygen functional groups (C=O peak at 1730 cm^{-1}, alcoholic C–OH peak at 1384 cm^{-1}, epoxide C–O–C or phenolic C–O–H stretching at 1225 cm^{-1}, C–O peak at 1066 cm^{-1}) had a significant decrease in the resultant TiO_2-rGO composites (Fig. 5-2) compared with the GO, suggesting the effective reduction of GO.

3.1.5. TG analysis

Thermal stability and quantified composition of the pure TiO_2 and TiO_2@rGO composites (10 wt%, 120 min irradiation) were analyzed via thermal gravity analysis. The experiments were performed from room temperature to 1000 °C in air flow at a heating rate of 10 °C/min.

As illustrated in Fig. 6, the pure P25 nanoparticles maintained generally stable with some small fluctuation, and TiO_2@rGO composites showed an obvious three-step weight loss: (1) weight loss about 0.39% below 100 °C was attributed to dehydration of physically adsorbed water molecules; (2) weight loss (1.35%) was observed at around 200 °C which was previously assigned to the removal of oxygenate groups on the surfaces of rGO; (3) the loss of weight (5.2%) above 300 °C occurred due to the removal of carbon sketch by burning of rGO [28,33]. Finally, TiO_2@rGO with the weight percent of 92% was left at 1000 °C when rGO was eventually burned up. Accordingly, the mass percentages of TiO_2 in TiO_2@rGO composite could be derived to be 92%. As the starting GO doping ratio was 10 wt%, the left TiO_2 amount could illustrate that the adding GO could be nearly fully attached and combined to TiO_2 nanoparticles during fabrication process, and the doping ratio could be simply regulated by GO addition.

3.1.6. UV–vis spectra

According to Fig. 7a-b, UV–vis diffuse reflectance spectroscopy was conducted to investigate the optical adsorption property of the obtained TiO_2@rGO composites that confirmed the prepared TiO_2@rGO compound could adsorb significantly more light in the 400–800 nm visible-light region, which was constant with the color change from white to black, as shown in the inset of Fig. 7a-b. The enhancement of absorption in the visible range increased with the augment of the GO additive amount in TiO_2@rGO composites as well as the irradiation duration. Notably, there was few differences between the adsorption of samples in 15 and 30 min UV irradiation duration and then an obvious enhancement in samples of 1 h and 2 h lasting irradiation could be observed, which illustrated that short time irradiation could hardly reduce the GO well and prolonging irradiation duration might contribute to the further reduction. Moreover, the bare TiO_2 exhibited a characteristic adsorption at about 390 nm, which was assigned to the intrinsic band gap absorption due to the electron transitions from the valence band to the conduction band ($O_{2p} \rightarrow Ti_{3d}$). From Fig. 7a-b, a gradual red shift to higher wavelength could be observed in the adsorption edge, which might be attributed to electronic interactions between rGO and TiO_2.

According to the Kubelka–Munk equation [34]:

$$F(R_\infty) = (1 - R_\infty)^2 / 2R_\infty \quad (1)$$

$$F(R_\infty) h\nu = C_1 \left(h\nu - E_g\right)^2 \quad (2)$$

Where $R = 10^{-A}$ and A is an optical adsorption, $h\nu$ is the photon energy and C_1 is a proportionality constant.

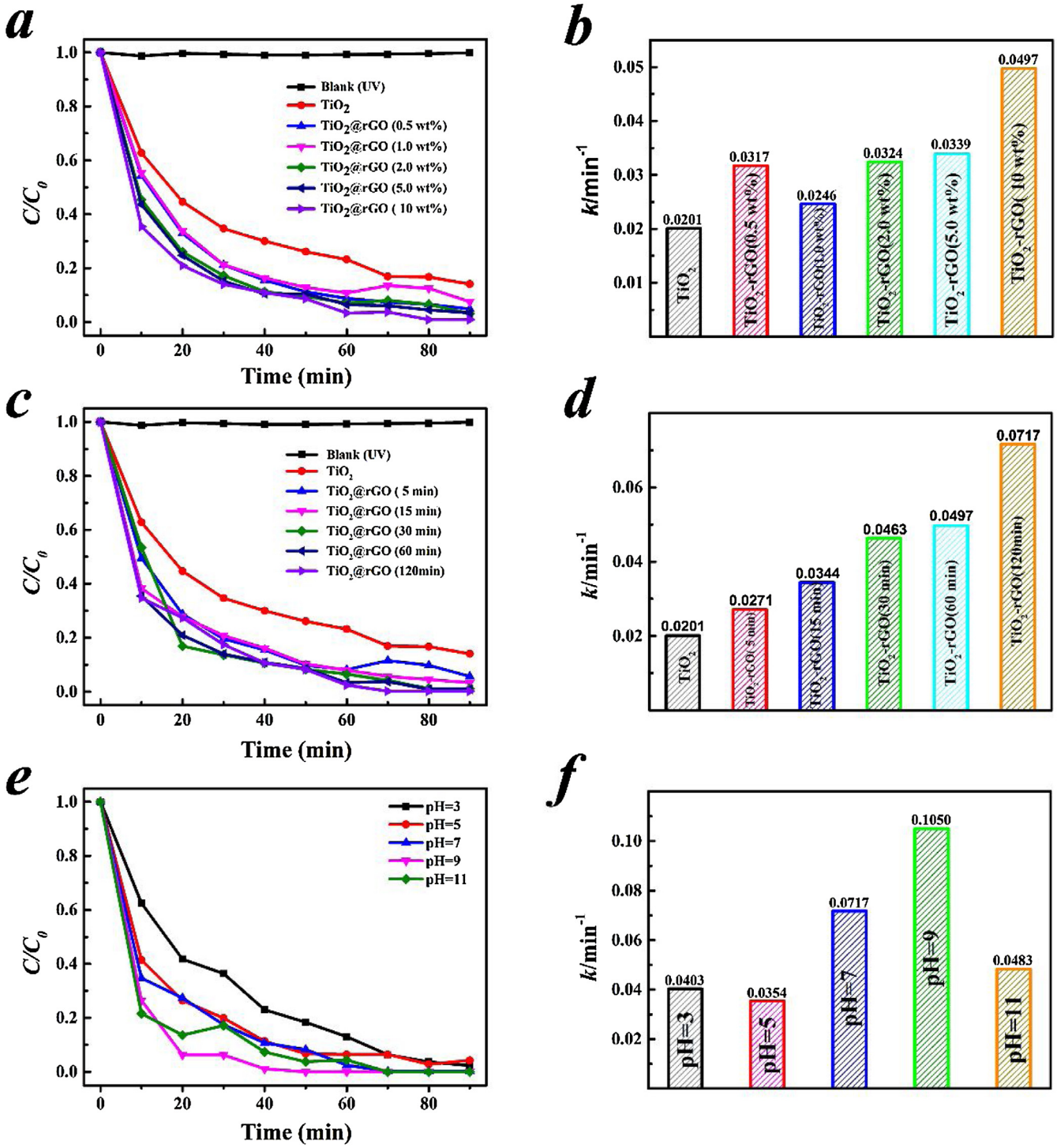

Fig. 9. Photocatalytic degradation of Rh 6G by pure TiO_2 and obtained TiO_2@rGO composites of various graphene doping ratio composites (a), different photo irradiation synthesizing time (c) and pH (e); and the apparent first-order rate constant (k) of as-prepared catalysts in Rh 6G decolouring: various graphene doping ratio composites (b), different photo irradiation synthesizing time (d) and in different pH circumstance (f), respectively.

The band gap of the obtained photocatalysts could be calculated from the equations. Fig. 7c plots the relationship of $[F(R_\infty)h\nu]^{1/2}$ versus photon energy, which showed that the band gap of pure TiO_2 was 3.08 eV, whereas the band gap of the prepared TiO_2@rGO composites of various graphene doping ratio and irradiation duration have been effectively reduced to 2.95 eV (0.5 wt%, 60 min irradiation), 2.87 eV (10 wt%, 5 min irradiation), 2.81 eV (10 wt%, 60 min irradiation) and 2.71 eV (10 wt%, 120 min irradiation), respectively. This variation could be interpreted as follows: during the UV-assisted photoreduction process, the functional groups on the surface of the prepared GO (eg. –OH, –COOH, and so on) have been reduced. Upon this situation, the π electron of the carbon atom did not entirely bond with others to form the delocalized large π bond, and some unpaired π electrons bonded with the free electrons on the surface TiO_2 to form a Ti–O–C structure, which then shifted up the valence band edge and reduced the band gap [35]. In combination process, the synergistic behavior of TiO_2 and graphene defined the composites as a "dyade" structure arising from the beneficial

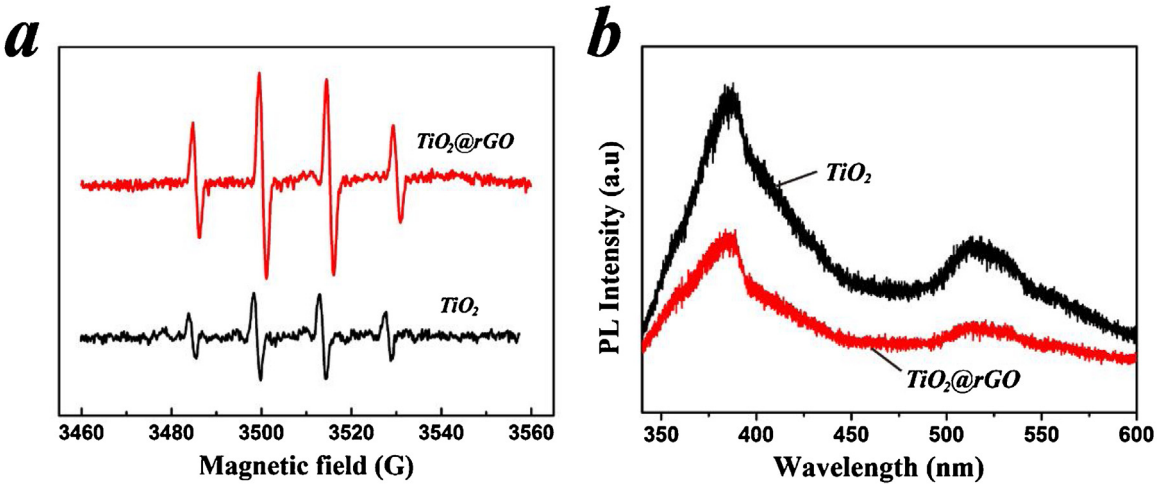

Fig. 10. (a) The hydroxyl radical EPR spectra of bare TiO_2 and TiO_2@rGO (10 wt%, 120 min irradiation) formed in aqueous dispersion in a pyrex vessel containing about 20 mg sample after 30 s irradiation by UV; (b) PL spectra of bare TiO_2 and the TiO_2@rGO composites (10 wt%) fabricated by 120 min.

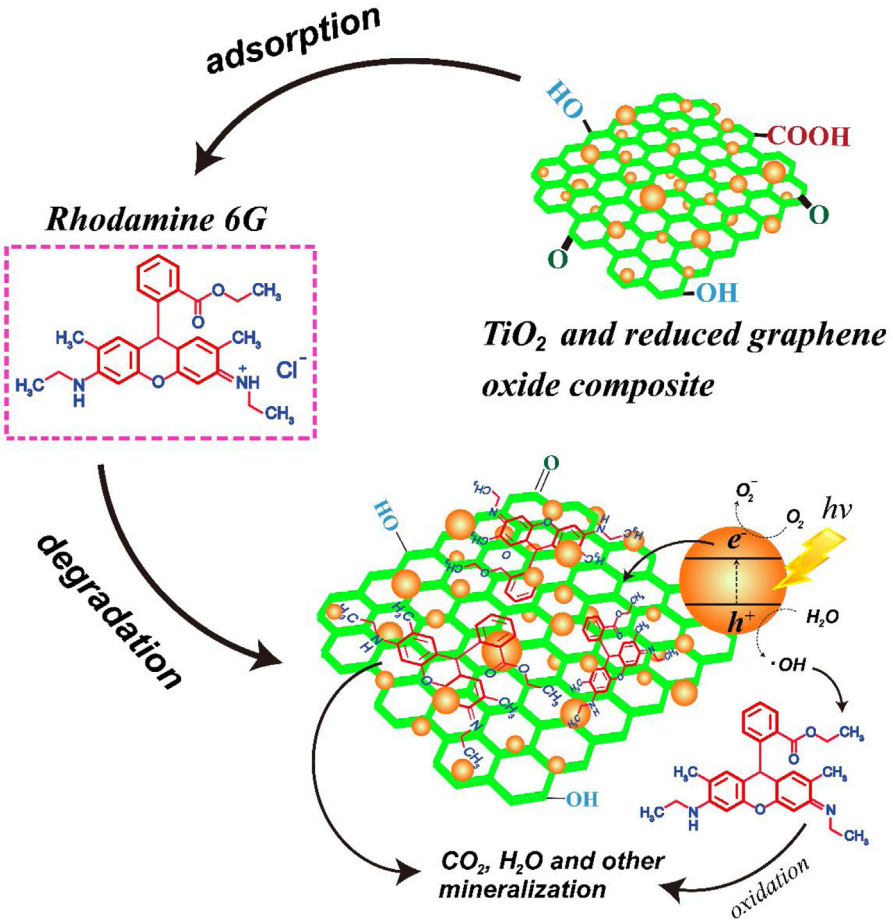

Fig. 11. Schematic illustration of Rh 6G decomposition through photodegradation by TiO_2@rGO composites.

interaction of the two. Namely, graphene and TiO_2 formed a joint electronic system. With increasing additive amount of graphene oxide, the TiO_2@rGO composites showed a continuously enhanced visible-light absorption in the range of 400–800 nm owing to the grafting of graphene, which was in agreement with the color change from white to black.

3.2. Adsorption and photocatalytic properties

3.2.1. Dye adsorption

The adsorption behavior of Rh 6G on the TiO_2@rGO with different doping ratios (0.5, 1.0, 2.0, 5.0, 10 wt%), various UV irradiation duration (5, 15, 30, 60, 120 min) and series of initial pH (3, 5, 7, 9, 11) have been investigated, as expressed in Fig. 7d–f. The target dye showed a slight adsorption towards pure TiO_2 (~5%). In contrast,

the incorporation of graphene significantly enhanced the adsorption of Rh 6G molecules on TiO_2@rGO nanocomposites surface.

To quantify the adsorption capacity of the obtained TiO_2@rGO composites, the Langmuir, Freundlich and Temkin adsorption isotherm models were applied to interpret the adsorption data. The theoretical parameters of adsorption isotherms along with regression coefficients were summarized in Table S1 (as expressed in Supporting Information).

In general, for the three isotherm models we applied, the result illustrated that the Langmuir equation was fitted better than the other two models, suggesting that the maximum adsorption capacities of TiO_2@rGO composites are gradually increasing with doping ratio raising.

According to Table 1, it illustrated that the adsorption enhancement was mainly owing to the improving doping ratio of GO which could effectively increase the specific surface area (as expressed in Table 2), as for 10 wt% TiO_2@rGO composites, about 91.8% of Rh 6G could be adsorbed within 30 min. However, upon to the UV irradiation duration which was another key factor in *in-situ* photoreduction method, there was little difference in adsorption capacities between a batch samples from 5 to 120 min due to the prolonging irradiation time had little to do with the specific surface area enhancement which stayed a quite important factor in adsorption process (as illustrated in Table 2).

Furthermore, the adsorption of the prepared compounds in a series of initial pH have been conducted either. The zero charge point(PZC) of TiO_2 was reported to be 6.3 previously [36]. In alkaline and acidic conditions, the titanium surface could be protonated or deprotonated. In other words, the TiO_2 surface would have positively charged when pH < PZC and negatively charged when pH > PZC. Moreover, as a typical cationic dye, Rh 6G would be ionized and positively charged. It meant that in relatively low pH range, there was a coulombic repulsion between the positive surface charged TiO_2 and the target dye. Thus leading to a relatively low adsorption at pH = 3, and Rh 6G adsorption gradually enhanced with the pH increasing (Fig. 7f). The adsorbability of TiO_2@rGO (10 wt%) reached its maximum when pH comes to 9, then facing a significant decrease at pH = 11.

This was due to the onium ion transformation in strong alkaline environment (pH > 10), as expressed in Fig. 8 [37,38]. Namely, the onium ion would transform into quaternary ammonium hydroxide and Rh 6G molecule would finally become electroneutral, so the electric attraction between TiO_2 (+) and dye would fade and disappear. Therefore, there was an apparent decline when pH reached at 11.

3.2.2. Dye photodecomposition

Since the graphene contents, irradiation duration and pH supposed to be the main significant factors in the catalysis of obtained TiO_2@rGO composites. The photocatalytic performance of TiO_2 and the prepared TiO_2@rGO composites have been evaluated by photocatalytic decolorization of Rh 6G aqueous solution

The normalized temporal concentration changes (*C/Co*) of Rh 6G during the photodegradation were proportional to the normalized maximum absorbance (*A/Ao*) and derived from the changes in Rh 6G's absorption profile (λ = 530 nm) at a given time interval. According to Fig. 9a, it was clear that all the TiO_2@rGO nanocomposites with a different doping ratio presented a better progress in the photodegradation of Rh 6G compared to the pure TiO_2, and it also exhibited the highest efficiency at the mass ratio of graphene:TiO_2 = 1:10. Under photocatalytic degradation process, about 65% Rh 6G has been decomposed by the TiO_2@rGO (10 wt%) in 10 min and the full degradation could be reached within 90 min which attributed to that more generated rGO could participate in transferring the photogenerated electrons of TiO_2. To further illustrated the enhancement, an apparent first-order equitation has been utilized:

$$Iog\left(\frac{C_0}{C}\right) = K_{app}t \quad (3)$$

Where K_{app} is the apparent first-order rate constant.

From Fig. 9b, all the TiO_2@rGO nanocomposites exhibited a higher photocatalytic activity than the pure TiO_2 ($k = 0.0201\ min^{-1}$) and the highest TiO_2@rGO (10 wt%) ($k = 0.0497\ min^{-1}$) was about 2.5 times as much as it. In addition, as a key factor in the *in-situ* photoreduction process, the photo irradiation duration effect on the photocatalytic activity of composites has been systematically discussed. According to Fig. 9c, a series of composites with different irradiation time from 5 to 120 min have been prepared which revealed a significant enhancement in Rh 6G degradation comparing to pure TiO_2. From Fig. 9d, it was clear that the enhancement of photocatalytic rate gradually increased with increasing irradiation duration. When the irradiation time got to 120 min, the rate reached its maximum ($k = 0.0717\ min^{-1}$) which was as 3.5 times as the rate of pure TiO_2. Thus proving that indeed a special performance was to be expected, due to the prolonging irradiation led the GO reduced more sufficiently and the excellent dyadic bonding between graphene and TiO_2 retarding the recombination of electron/hole pairs, which was confirmed by the XPS and PL spectra (as expressed in Fig. 10b). Furthermore, the solution pH played an important role in the photocatalytic degradation process of various pollutants. The effect of pH on the photodegradation of Rh 6G has been studied in the pH range 3–11. The pH of the solution was adjusted before irradiation and it was not controlled during the course of the reaction. The effect of initial pH on degradation was shown in Fig. 9e-f. Furthermore, the solution pH also determined the surface charge properties of TiO_2, the size of aggregates formed, the charge of Rh 6G molecules, adsorption of dyes onto TiO_2@rGO surface, and the concentration of hydroxyl radicals. The *pseudo*-first order rate constants for TiO_2@rGO at pH 3, 5, 7, 9 and 11 were 0.0403, 0.0354, 0.0717, 0.1050 and $0.0483\ min^{-1}$, respectively. From the experimental results the photocatalytic degradation efficiency of TiO_2@rGO was observed to be higher at alkalescent pH = 9, which was be identical to maximum adsorption observed at pH = 9 either. Hence, the higher degradation efficiency was mainly due to the strong adsorption of Rh 6G on the catalyst surface.

3.3. Mechanism of degradation

The production of •OH radicals in the reaction system could be detected by the electron paramagnetic resonance (EPR) spin trap technique[39,40], using 5,5-dimethyl-1-pyrroline-N-oxide (DMPO) as the spin-trapping reagent. The result was shown in Fig. 10a. It was clear that the characteristic 1:2:2:1 spectral peaks of DMPO-•OH adducts for bare TiO_2 and TiO_2@rGO (10 wt%, 120 min irradiation) samples could be observed, which illustrated that •OH radicals have been generated on the surface of both samples. Additionally, the intensity of the peaks of the obtained composites was obviously stronger than that of pure TiO_2. Thus, the amount of •OH radicals produced on the surface of TiO_2@rGO (10 wt%, 120 min irradiation) was more than that of pure TiO_2. Therefore, the TiO_2@rGO composites was photocatalytically more active than TiO_2 nanoparticles. It could be inferred that Rh 6G were eliminated mainly by means of •OH radical oxidation under UV irradiation.

Moreover, the PL emission spectra were employed to investigate the combination and separation of the photoinduced carriers. The stronger the PL intensity was, the faster the photoexcited h^+/e^- combined. Generally, a higher PL intensity indicated a higher recombination rate and a lower PL intensity expressed a lower recombination rate. According to Fig. 10b, the PL peak around 400 nm was a result of the transition from localized surface states

Table 1
Adsorption capacities of prepared TiO_2@rGO composites.

	Doping ratio (%)					Irradiation time (min)				
parameter	0.5	1.0	2.0	5.0	10	5	15	30	60	120
q_m (mg/g)	1.5	1.4	4.1	15.4	35.2	34.6	32.7	32.9	35.2	36.4

Table 2
The specific surface area of pure TiO_2 and obtained TiO_2@rGO composites.

	TiO_2	TiO_2@rGO (60 min)	TiO_2@rGO (120 min)
specific surface area (m^2/g)	49.958	78.4874	79.1349

to the valance band of TiO_2 and the peak around 500 nm was owing to the transition from localized surface states to the valance band of TiO_2. It was obvious that the obtained TiO_2@rGO composites showed a decrease in intensity, which might attribute to inhibition of the h^+/e^- recombination.

Based on what has been observed and discussed above, the superior performance of TiO_2@rGO composites in the decomposition of Rh 6G could be attributed to the positive synergistic effect of graphene and TiO_2 nanoparticles. Firstly, cationic Rh 6G molecules could be easily attached to the surfaces of rGO by three approaches: electrostatic attraction as well as π-π conjugation based on the negatively charged structure, part π-conjugation system and the great specific surface area. Such adsorption enhancement increased the effective concentration of Rh 6G molecules significantly near the surfaces of the TiO_2@rGO composites, resulting in high catalytic degradation rate. Then, the hydrophilic functional groups on rGO led to the well dispersion of TiO_2@rGO composite in liquid phase, thus improving the wettability of the catalyst in aqueous solution. Moreover, excellent contact between TiO_2 nanoparticles and rGO sheets also prevented TiO_2 from leaching out in the catalytic reactions, then efficiently generating free •OH radical species and eventually facilitated the degradation of Rh 6G molecules. Fourth, due to the excellent conductivity of graphene, the electron/hole recombination could be inhibited and extend the h^+ existence time. Finally, on account of the strong oxidizability of free •OH radicals, the target Rh 6G molecule could be transformed to CO_2, H_2O and some small molecules that would be desorbed from the TiO_2, thus the graphene surface and the active sites could be effectively recovered. Therefore, there would be a synergy between adsorption and catalytic reaction in the process for TiO_2@rGO composite, resulting in an appreciable improvement in decomposition of organic pollutant compared with bare TiO_2 (Fig. 11).

4. Conclusion

In summary, based on UV-assisted photoreduction strategy, GO could be effectively reduced via a facile and green strategy without using any reducing agents and TiO_2@rGO composites of different graphene doping ratio and various UV irradiation duration have been *in-situ* synthesized simultaneously. The results showed all resultant TiO_2@rGO composites performed better in photodegrading rhodamine 6G imitated wastewater than the commercial P25 nanoparticles, which illustrated that the additive reduced graphene oxide (rGO) could be used as an effective co-catalyst to improve the photocatalytic performance of TiO_2 as an effective transfer and separation of photogenerated electrons and holes. Regarding to photocatalytic ability, TiO_2@rGO (10 wt%, 120 min irradiation) was observed to be the optimum sample which showed a 3.5 times enhancement for rhodamine 6G photodegradation process than bare P25 nanoparticles. Considering the green and effective method for the synthesis of TiO_2@rGO composites, this work may provide a facile, promising, and environmentally friendly strategy for the large-scale preparation of graphene-based composite materials.

Conflict of interests

The authors declare that there is no conflict of interests regarding the publication of this paper. S.Y. Pu and R. Zhu. contributed equally to this work.

Acknowledgments

This work was supported by the National Natural Science Foundation of China (51408074) and the Research Fund of State Key Laboratory of Geohazard Prevention and Geoenvironment Protection (Nos. SKLGP2015Z007, SKLGP2017Z009). Dr. S.Y. Pu is grateful for support from the Hong Kong Scholars Program (No. XJ2015005 and G-YZ80) and the Project Funded by China Postdoctoral Science Foundation (2015T80966).

Appendix A. Supplementary data

Supplementary data associated with this article can be found, in the online version, at http://dx.doi.org/10.1016/j.apcatb.2017.06.039.

References

[1] W. Wei, D. Liu, Z. Wei, Y. Zhu, Short-range π-π stacking assembly on P25 TiO2 nanoparticle for enhanced visible-light photocatalysis, ACS Catal. 7 (2017) 652–663.
[2] W.J. Jiang, Y.F. Liu, J. Wang, M. Zhang, W.J. Luo, Y.F. Zhu, Separation-free Polyaniline/TiO2 3D hydrogel with high photocatalytic activity, Adv. Mater. Interfaces 3 (2016) 9.
[3] T. Tatsuma, S. Saitoh, Y. Ohko, A. Fujishima, TiO2- WO3 photoelectrochemical anticorrosion system with an energy storage ability, Chem. Mater. 13 (2001) 2838–2842.
[4] C.P. Sajan, S. Wageh, A.A. Al-Ghamdi, J.G. Yu, S.W. Cao, TiO2 nanosheets with exposed {001} facets for photocatalytic applications, Nano Res. 9 (2016) 3–27.
[5] X. Chen, S.S. Mao, Titanium dioxide nanomaterials: synthesis, properties, modifications, and applications, Chem. Rev. 107 (2007) 2891–2959.
[6] H. Tong, S.X. Ouyang, Y.P. Bi, N. Umezawa, M. Oshikiri, J.H. Ye, Nano-photocatalytic materials: possibilities and challenges, Adv. Mater. 24 (2012) 229–251.
[7] Z. Zhang, C.-C. Wang, R. Zakaria, J.Y. Ying, Role of particle size in nanocrystalline TiO2-based photocatalysts, J. Phys. Chem. B 102 (1998) 10871–10878.
[8] W.K. Wang, J.J. Chen, M. Gao, Y.X. Huang, X. Zhang, H.Q. Yu, Photocatalytic degradation of atrazine by boron-Doped TiO2 with a tunable Rutile/Anatase ratio, Appl. Catal. B Environ. 195 (2016) 69–76.
[9] R.R. Hao, G.H. Wang, H. Tang, L.L. Sun, C. Xu, D.Y. Han, Template-free preparation of macro/mesoporous g-C3N4/TiO2 heterojunction photocatalysts with enhanced visible light photocatalytic activity, Appl. Catal. B Environ. 187 (2016) 47–58.
[10] N. Bouazza, M. Ouzzine, M.A. Lillo-Rodenas, D. Eder, A. Linares-Solano, TiO2 nanotubes and CNT-TiO2 hybrid materials for the photocatalytic oxidation of propene at low concentration, Appl. Catal. B Environ. 92 (2009) 377–383.
[11] K. Woan, G. Pyrgiotakis, W. Sigmund, Photocatalytic carbon-nanotube-TiO2 composites, Adv. Mater. 21 (2009) 2233–2239.
[12] Q.J. Xiang, J.G. Yu, M. Jaroniec, Graphene-based semiconductor photocatalysts, Chem. Soc. Rev. 41 (2012) 782–796.

[13] A.K. Geim, K.S. Novoselov, The rise of graphene, Nat. Mater. 6 (2007) 183–191.
[14] M.I. Katsnelson, K.S. Novoselov, Graphene New bridge between condensed matter physics and quantum electrodynamics, Solid State Commun. 143 (2007) 3–13.
[15] W.J. Jiang, Y.F. Zhu, G.X. Zhu, Z.J. Zhang, X.J. Chen, W.Q. Yao, Three-dimensional photocatalysts with a network structure, J. Mater. Chem. A 5 (2017) 5661–5679.
[16] X. Pan, Y. Zhao, S. Liu, C.L. Korzeniewski, S. Wang, Z. Fan, Comparing graphene-TiO2 nanowire and graphene-TiO2 nanoparticle composite photocatalysts, ACS Appl. Mater. Interfaces 4 (2012) 3944–3950.
[17] J.S. Lee, K.H. You, C.B. Park, Highly photoactive, low bandgap TiO2 nanoparticles wrapped by graphene, Adv. Mater. 24 (2012) 1084–1088.
[18] N. Li, G. Liu, C. Zhen, F. Li, L. Zhang, H.M. Cheng, Battery performance and photocatalytic activity of mesoporous anatase TiO2 nanospheres/graphene composites by template-free self-assembly, Adv. Funct. Mater. 21 (2011) 1717–1722.
[19] H. Zhang, X. Lv, Y. Li, Y. Wang, J. Li, P25-graphene composite as a high performance photocatalyst, ACS Nano 4 (2010) 380–386.
[20] Y. Liang, H. Wang, H.S. Casalongue, Z. Chen, H. Dai, TiO2 nanocrystals grown on graphene as advanced photocatalytic hybrid materials, Nano Res. 3 (2010) 701–705.
[21] G. Williams, B. Seger, P.V. Kamat, TiO2-graphene nanocomposites. UV-assisted photocatalytic reduction of graphene oxide, ACS Nano 2 (2008) 1487–1491.
[22] H. Zhang, X. Liu, G. He, X. Zhang, S. Bao, W. Hu, Bioinspired synthesis of nitrogen/sulfur co-doped graphene as an efficient electrocatalyst for oxygen reduction reaction, J. Power Sources 279 (2015) 252–258.
[23] A.L. Linsebigler, G. Lu, J.T. Yates, Photocatalysis on TiO2 surfaces: principles, mechanisms, and selected results, Chem. Rev. 95 (1995) 735–758.
[24] H.A. Becerril, J. Mao, Z. Liu, R.M. Stoltenberg, Z. Bao, Y. Chen, Evaluation of solution-processed reduced graphene oxide films as transparent conductors, ACS Nano 2 (2008) 463–470.
[25] N.A. Kotov, I. Dékány, J.H. Fendler, Ultrathin graphite oxide–polyelectrolyte composites prepared by self-assembly: transition between conductive and nonéconductive states, Adv. Mater. 8 (1996) 637–641.
[26] M.-Q. Yang, N. Zhang, Y.-J. Xu, Synthesis of fullerene-, carbon nanotube-, and graphene-TiO2 nanocomposite photocatalysts for selective oxidation: a comparative study, ACS Appl. Mater. Interfaces 5 (2013) 1156–1164.
[27] E. Papirer, R. Lacroix, J.-B. Donnet, G. Nansé, P. Fioux, XPS study of the halogenation of carbon black—Part 2. Chlorination, Carbon 33 (1995) 63–72.
[28] G. Park, L. Bartolome, K.G. Lee, S.J. Lee, T.J. Park, One-step sonochemical synthesis of a graphene oxide–manganese oxide nanocomposite for catalytic glycolysis of poly (ethylene terephthalate), Nanoscale 4 (2012) 3879–3885.
[29] V. Abdelsayed, S. Moussa, H.M. Hassan, H.S. Aluri, M.M. Collinson, M.S. El-Shall, Photothermal deoxygenation of graphite oxide with laser excitation in solution and graphene-aided increase in water temperature, J. Phys. Chem Lett. 1 (2010) 2804–2809.
[30] D. Wang, Y. Li, Q. Wang, T. Wang, Nanostructured Fe2O3–graphene composite as a novel electrode material for supercapacitors, J. Solid State Electrochem. 16 (2012) 2095–2102.
[31] J. Shen, T. Li, Y. Long, M. Shi, N. Li, M. Ye, One-step solid state preparation of reduced graphene oxide, Carbon 50 (2012) 2134–2140.
[32] C. Hou, Q. Zhang, Y. Li, H. Wang, P25–graphene hydrogels: room-temperature synthesis and application for removal of methylene blue from aqueous solution, J. Hazard. Mater. 205 (2012) 229–235.
[33] Y.Q. Li, J.Y. Qu, F. Gao, S.Y. Lv, L. Shi, C.X. He, J.C. Sun, In situ fabrication of Mn3O4 decorated graphene oxide as a synergistic catalyst for degradation of methylene blue, Appl. Catal. B Environ. 162 (2015) 268–274.
[34] L. Wan, J. Li, J. Feng, W. Sun, Z. Mao, Anatase TiO 2 films with 2.2 eV band gap prepared by micro-arc oxidation, Mater. Sci. Eng.: B 139 (2007) 216–220.
[35] Y. Zhang, C. Pan, TiO2/graphene composite from thermal reaction of graphene oxide and its photocatalytic activity in visible light, J. Mater. Sci. 46 (2011) 2622–2626.
[36] N. Jaffrezic-Renault, P. Pichat, A. Foissy, R. Mercier, Effect of deposited Pt particles on the surface charge of TiO/sub 2/aqueous suspensions by potentiometry, electrophoresis, and labeled ion adsorption, J.Phys. Chem. (United States) 90 (1986).
[37] E. Hughes, C. Ingold, C. Patel, 135. Influence of poles and polar linkings on the course pursued by elimination reactions. Part XVI. Mechanism of the thermal decomposition of quaternary ammonium compounds, J. Chem. Soc. (Resumed) (1933) 526–530.
[38] C.A. Deakyne, M. Meotner, Unconventional ionic hydrogen bonds. 2. NH+.cntdot.cntdot.cntdot.pi. Complexes of onium ions with olefins and benzene derivatives, J. Am. Chem. Soc. 107 (1985) 474–479.
[39] S. Chen, Y. Hu, S. Meng, X. Fu, Study on the separation mechanisms of photogenerated electrons and holes for composite photocatalysts g-C 3 N 4 −WO 3, Appl. Catal. B Environ. s150–s151 (2014) 564–573.
[40] X. Fu, Y. Hu, Y. Yang, W. Liu, S. Chen, Ball milled h-BN: an efficient holes transfer promoter to enhance the photocatalytic performance of TiO_2, J. Hazard. Mater. 244–245 (2013) 102.